Exp Fluids (2009) 47:827–838
DOI 10.1007/s00348-009-0727-1

RESEARCH ARTICLE

Investigation of vortex dynamics downstream of moving leaflets using robust image velocimetry

Giovanni P. Romano · Giorgio Querzoli · Massimo Falchi

Received: 2 October 2008 / Revised: 29 July 2009 / Accepted: 30 July 2009 / Published online: 16 September 2009

Abstract The interaction of a sudden flow through a rectangular slot with moving leaflets, hinged at its border, was investigated experimentally in a Plexiglas vessel. This configuration resembles schematically some key features of many biological flows, e.g. in sea-animal propulsion, where the moving flaps control the flow, optimizing thrust, or in heart valves, where leaflets prevent backflow. Therefore, the comprehension of the basic mechanisms of the flow-structure interaction and of the features of the flow is of interest in a wide range of applications. Although some detail of the phenomenon could depend on the specific leaflet design, material and forcing, the objective of the present work is to investigate the overall dependence of the flow field on the leaflet arrangement. Specifically, three leaflet configurations have been tested at Reynolds number $Re = 2{,}000$ and Strouhal number $St = 0.2$: two symmetrical leaflets, two non-symmetrical leaflets, one being twice as wide as the other, and a single leaflet. Velocity fields were obtained using Robust Image Velocimetry in order to accurately resolve the structure of the vorticity field. The dynamics of the opening leaflets, the vorticity fields and the features of the vortices generated during the leaflet opening were investigated and compared in the different leaflet configurations. Advantages in the opening time, maximum aperture and closing time were observed in the two-leaflet non-symmetrical case in comparison to the other configurations.

G. P. Romano (✉)
Department of Mechanics and Aeronautics,
University "La Sapienza", Rome, Italy
e-mail: romano@dma.ing.uniroma1.it

G. Querzoli
Dipartimento di Ingegneria del Territorio,
University of Cagliari, Cagliari, Italy

M. Falchi
INSEAN, Italian Ship Model Basin, Rome, Italy

1 Motivations

The sudden onset of a jet-flow, released in calm ambient, generates a starting vortex ring that begins to travel in the direction of the jet axis. The circulation increases up to a limiting value and, if the starting vortex is further fed up, the pinch-off occurs, and the trailing jet does not contribute anymore to the increase in circulation of the vortex, producing a vorticity layer in its wake (Dabiri and Gharib 2005a, b). The interaction between a sudden flow and moving leaflets is common in several flows. Examples can be found in the flow through cardiac valves (Brucker et al. 2002; Akutsu et al. 2005; Kaminsky et al. 2007) or in aquatic animal propulsion (Anderson and Grosenbaugh 2005). The characteristics of the jet-flow play a fundamental role in the features of the resulting vortex ring; for this reason, many investigations have been conducted in the past (in Shariff and Leonard 1992, a comprehensive review is given). To be mentioned is the work of Saffman (1970), who laid down the theoretical framework to predict the travel velocity of a viscous vortex ring, and the one of Pullin (1979), using similarity theories to predict the main parameters of vortex rings originated from sudden flows both through tubes and orifices. On the basis of experimental observations, Gharib et al. (1998) suggested an analytical model describing a parameter limiting the growth of a vortex ring and the consequent pinch-off. Some investigators also considered variable diameter orifices, extending to those cases the time scaling originally

proposed for the pipes and orifices (Dabiri and Gharib 2005a, b).

When the jet-flow is coupled with moving leaflets, the vortex generation is driven by the developing boundary layer on the leaflet surface, and it is highly influenced by the specific leaflet geometry. Almost all experimental and numerical approaches consider axial-symmetry as the basis to investigate the phenomenon and also the design of prosthetic valves preserves some rotational symmetry (valves with two and three leaflets). Recent three-dimensional direct numerical simulation (DNS) of the entire aortic root geometry with prosthetic bileaflet valves well reproduced in vitro results (Dasi et al. 2007; De Tullio et al. 2009). Nevertheless, as always in nature, symmetries are only ideal simplifications. It has been reported that the left ventricle, aortic root and valves are parts of a highly non-symmetric complex system (Grande et al. 1998, Cooke et al. 2004). Although this asymmetry may influence the valvular mechanics, the resulting tissue dilatation and bioprosthetic valve durability, it was rarely considered in previous experimental and numerical valve models.

Bolzon et al. (2003), inspired by the asymmetric position of the mitral valve in the left ventricle of the human heart, investigated the effect of the asymmetry on the flow through an orifice in a pipe. They observed that the asymmetry modulates the intensity of the vortex ring, producing a smaller and weaker vortex on the side close to the wall. They concluded that the asymmetry of the mitral valve facilitates the ejection through the aorta during ventricular contraction. However, the non-symmetrical nature of the left-ventricular flow also originates from an asymmetry of the mitral valve, which consists of two leaflets of different size. The jet configuration that derives from the asymmetric leaflets affects the shape of the vortex ring and the corresponding different intensity of the vorticity on the two sides. Moreover, the presence of only two leaflets in the mitral valve leads to the possibility of understanding the main features of the phenomenon by means of two-dimensional investigations. Pedrizzetti and Domenichini (2006) simulated numerically the phenomenon, but experimental investigations are, to the extent of our knowledge, still missing.

On this path, the present experimental investigation reproduces in the laboratory some of the above-mentioned asymmetries, though in a very schematic geometry, in order to point out the main features of the interaction between starting flow and moving leaflets. With this aim, the flow downstream of a thin edge rectangular orifice was investigated (the orifice geometry was selected to obtain a nearly two-dimensional flow and characterized by two counter-rotating vortices). The fluid motion was generated by a piston driven by a gradually varying velocity programme. The orifice was equipped with rectangular leaflets hinged on its sides. The leaflets were as high as the orifice and together were able to occlude the orifice completely. The velocity and vorticity fields resulting from the earlier mentioned configurations were measured in time over different piston cycles by means of robust image velocimetry (RIV), which is a sort of Particle Image Velocimetry where the dissimilarity between interrogation windows is evaluated by means of a robust estimator (Falchi et al. 2006).

2 Experimental set-up and procedures

The set-up includes a circular piston (10.0 cm in diameter) driven by a linear motor that forces the water flow to generate a jet through a thin edge rectangular orifice (height, $H = 40$ cm, and width, $D = 3.0$ cm, Fig. 1). Rectangular leaflets are hinged on the sides of the orifice by means of (thin) adhesive tape stuck on their downstream face. The leaflets were made of 1.4-mm thick aluminium. The tape avoided leakage between the side of the orifice and the leaflet. As a consequence of the forward motion of the piston, the water jet forces the leaflets to open and flows though the orifice, thus generating a couple of counter-rotating vortices. The position of each of the two leaflets is described by the aperture angle θ, i.e. the angle between each leaflet and the wall plane. This angle is defined in Fig. 2. Three configurations with different index of symmetry, $\varepsilon = l_1/l_2$, have been investigated [l_1 and l_2 denote the width of the small and large leaflets, respectively (Fig. 2)]:

1. symmetric: two leaflets of the same width ($\varepsilon = 1$);
2. asymmetric: two leaflets of different widths ($\varepsilon = 0.5$);
3. single: one leaflet as wide as the orifice ($\varepsilon = 0$).

A honeycomb in the upstream chamber avoided the formation of large vortical structures due to the piston motion before the flow enters into the second chamber

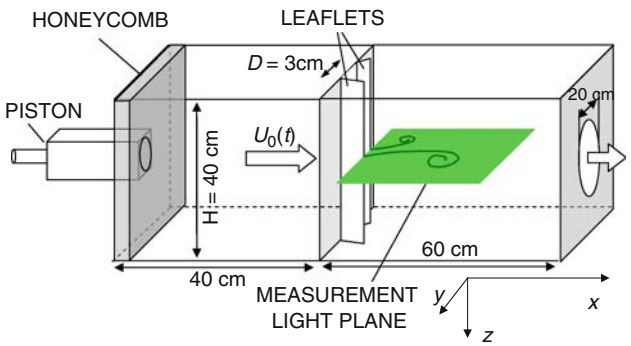

Fig. 1 The moving leaflet jet apparatus with coordinate system

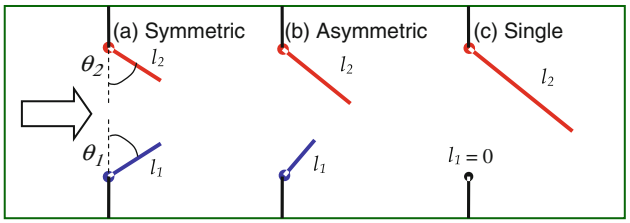

Fig. 2 The three tested leaflet configurations on the test plane with leaflet aperture angles

(dimensions: 40 × 40 × 40 cm) through the orifice. The fluid flowed out of the second chamber through a centred circular orifice, 20 cm in diameter. As the piston reaches the maximum velocity and starts to decelerate, the leaflets get the maximum aperture angle and from then on, the closure phase starts. The details of this process are dependent on the specific forcing curve assigned to the piston, which is feedback-controlled in position by a computer. During the present measurements, the piston moved forward with a cosinusoidal ramp of the form:

$$S(t) = A[1 - \cos(\pi t/T_e)]/2,$$

where $S(t)$ indicates the piston displacement, A the stroke volume and $T_e = 0.56$ s the duration of the ascending ramp. The stroke was tuned to obtain a stroke volume of 250 ml. Then, the piston remained at rest for a time interval $T_r = 1.12$ s, and finally returned to the initial position with a slow backward sinusoidal ramp. The duration of the entire cycle was $T = 5$ s. The above described time law allows the continuity of displacement, velocity and acceleration of the piston at the end of the ascending ramp. The resulting Reynolds number, $Re = U_0 d/\nu$, and Strouhal number, $St = d/(U_0 T_e)$, were equal to 2,000 and 0.2, respectively (U_0 indicates the peak velocity, $d = D/2$ the orifice semi-aperture and ν the kinematic viscosity of the water). These values are in the typical range of mitral valve dynamics.

The measuring horizontal plane, placed at half the height of the test section, was illuminated by a 5.5 W continuous laser, generating a 2-mm thick light sheet with a uniform in-plane light distribution and depth over the 10 cm span of the measuring area. Series of images were taken from the top using a high-speed Photron camera that was able to acquire up to 2,000 images per second at the full resolution of 1,024 × 1,024 pixels × 8 bits. The camera was triggered by the piston motion so that images could be acquired repeatedly at the same points of the cycle. For each cycle, 75 phases were considered, and the acquisitions were repeated 60 times in order to compute phase averages. The water in the whole apparatus was seeded with non-buoyant, hollow-glass spherical particles 10 μm in diameter.

Images were processed using the robust image velocimetry (RIV) algorithm, in which the particle displacements between consecutive images are found by minimizing the dissimilarity between interrogation windows evaluated by means of robust statistics (the Lorentzian operator). The RIV algorithm uses pyramidal filtering to capture large particle displacements as well as Gaussian sub-pixel interpolation to get sub-pixel resolution. This technique was chosen due to its high accuracy in resolving the small-scale structure of the vorticity field. Further details and comparison to PIV are given in Falchi et al. (2006). Examples of the acquired images in the three leaflet configurations are shown in Fig. 3. The generated vortex structure is clearly visible as well as the leaflet positions due to reflected light, although the leaflets were painted in black.

In order to characterize the mechanical properties of the hinge, the ratio, K, of the closing torque per unit length generated by the tape to the opening angle of the leaflet was measured for increasing angles, θ. The quantity K is plotted in Fig. 4 as a function of the opening angle, normalized by the complete aperture $\pi/2$. As a consequence, the normalized angle ranges from zero (leaflet closed) up to one (leaflet completely open). K is steeply increasing with the aperture up to a normalized angle of 0.25. Increasing further the aperture, K oscillates around a nearly constant value ($K_0 = 4.41$ mN/m^2/rad).

Using dimensional analysis arguments, the ratio of fluid dynamic torque to hinge torque can be estimated of order:

$$\frac{\rho U_0^2 D^2}{K_0 \theta_0} \approx 4.2;$$

where ρ is the fluid density, and $\theta_0 \cong 0.87$ is a maximum aperture angle. As a consequence, the torque generated by the tape may affect the dynamics of the leaflet for large angles, in particular influencing the maximum aperture of the leaflets. However, the plot of Fig. 4 suggests that the effect of the torque generated by the tape may be negligible at the beginning of the motion, when the leaflets are nearly closed, because the torque is very low at small angles.

Similar dimensional arguments yield an estimate of the ratio of fluid dynamic torque to the variation of angular momentum of the leaflets:

$$\frac{\rho U_0^2 D^2}{\rho_a I \dot{\omega}} \approx 3\frac{\rho}{\rho_a} U_0 T_e = 59.2$$

where ρ_a is the leaflet mass per unit area, $\dot{\omega} \approx U_0/(DT_e)$ the time derivative of the angular velocity, $I = D^3/3$ the moment of inertia, per unit length, of the leaflet. On this basis, it is reasonable to assume that the inertia of the leaflets does not affect significantly the phenomenon.

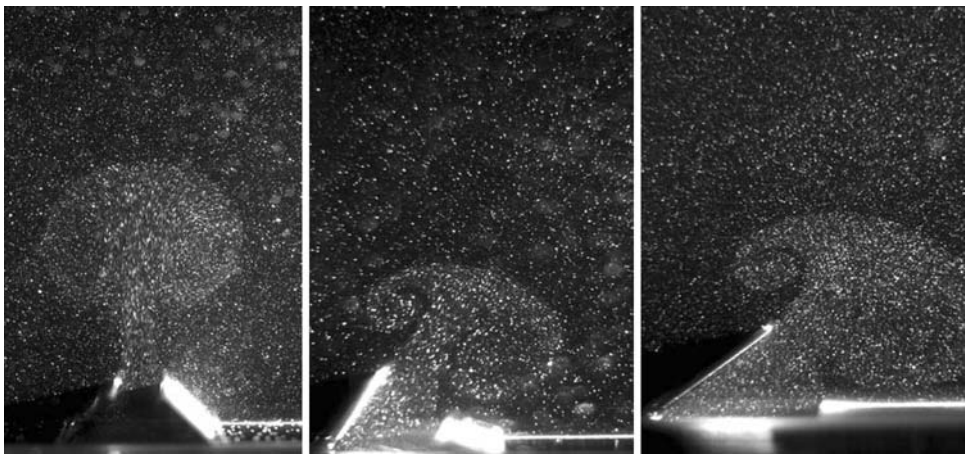

Fig. 3 Image acquisition in different leaflet configurations: two symmetrical leaflets on the *left* ($\varepsilon = 1.0$), two non-symmetrical leaflets in the *centre* ($\varepsilon = 0.5$) and a single leaflet on the *right* ($\varepsilon = 0.0$)

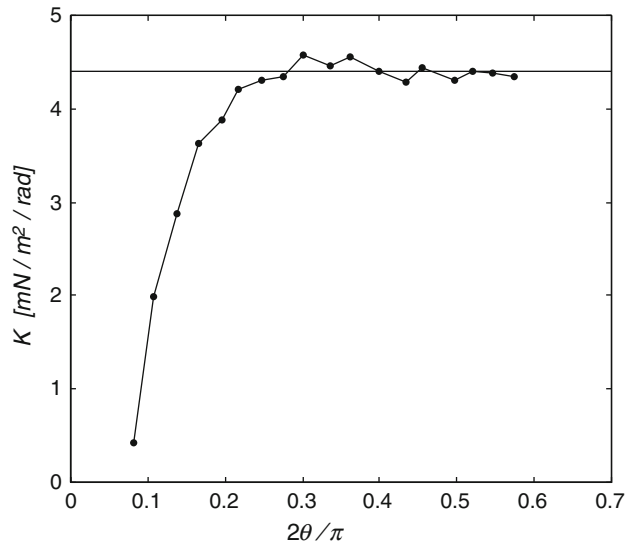

Fig. 4 Ratio of the torque per unit length of the hinge to the leaflet opening angle, K, vs. the normalized opening angle. The *horizontal reference line* indicates the average value, K_0, of the last nine measured values

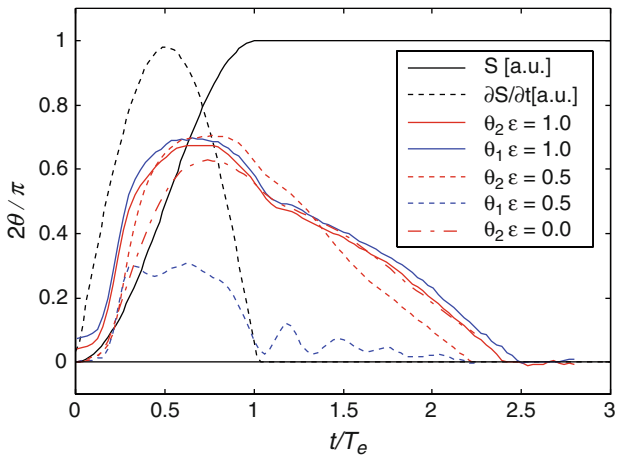

Fig. 5 Piston position and velocity in time (arbitrary vertical units) with leaflet angular positions in the different configurations. Left leaflets are indicated in *red* and right leaflets in *blue*

3 Results

To understand the phenomenon of vortex generation and propagation, it is very important to describe in detail the temporal leaflet positions in comparison to the forcing piston position and velocity. This relation is shown in Fig. 5. As soon as the piston starts to move, and the velocity becomes significant, the leaflets start to open very similarly in the different configurations (as indicated in Fig. 2, the #2 indicates the left leaflet, i.e. the one generating a vortex with positive vorticity, whereas the #1 indicates the right leaflet i.e. the one generating negative vorticity). The initial angle is slightly positive ($\theta \approx 0.05\pi/2$) only for $\varepsilon = 1.0$, possibly due to a non-perfect closure at the end of the previous cycle. Moreover, a significant delay in the aperture time in the single-leaflet configuration is noticed. However, this initial delay does not cause large differences in the time when the aperture angle is a maximum ($t/T_e \approx 0.8$), except for the small leaflet of the case $\varepsilon = 0.5$. The two leaflets of the case $\varepsilon = 0.5$ move with almost perfect symmetry until $t/T_e \approx 0.30$, when the small leaflet reaches its maximum aperture ($\theta \approx 0.27\pi/2$). Afterwards, the long leaflet continues to open, whereas the short leaflet remains about at the same angle for a time interval $0.4T_e$ long. Then, it tends to close again and begins to oscillate with a period of $0.3T_e$. Though the focus of the present investigation is only on the effects of the leaflets configurations, further measurements have been performed in order to clarify whether the oscillations are the consequence of a particular condition of resonance, or can be interpreted as general behaviour, due to the ratio of the sizes of the leaflets. In Fig. 6, the small leaflet angle has been plotted, as a function of time, by varying both the Reynolds and the Strouhal numbers. The features of the plots are quite similar, with a plateau after reaching the maximum aperture and oscillations with

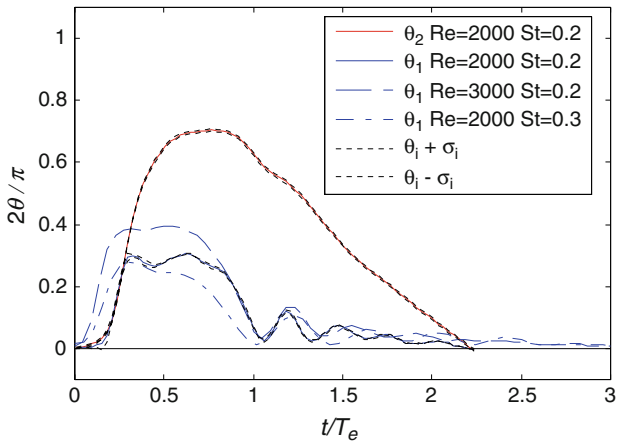

Fig. 6 Confidence intervals (*dotted lines*) of the opening angle of leaflet #1 (*blue line*) and #2 (*red line*) for non-symmetric leaflets ($\varepsilon = 0.5$). *Dashed and dash/dotted lines* indicate the angle of the short leaflet at $Re = 3{,}000$, $St = 0.2$ and $Re = 2{,}000$, $St = 0.3$, respectively

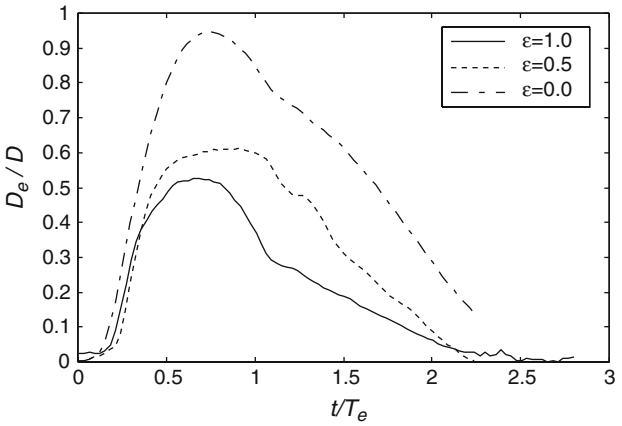

Fig. 7 Effective leaflet aperture, D_e, non-dimensionalized by the orifice width as a function of the non-dimensional time

similar amplitude and period. As a consequence, the behaviour described earlier can be considered as typical of the index of symmetry, $\varepsilon = 0.5$.

Figure 5 indicates that the maximum velocity is reached at $t/T_e \approx 0.25$ in all cases, excluding the short leaflet at $\varepsilon = 0.5$, which reaches the maximum velocity at $t/T_e \approx 0.27$. The maximum aperture angle is attained by the long leaflet for $\varepsilon = 0.5$. The reason for this is that the fluid exiting from the orifice is deflected by the short leaflet towards the opposite leaflet, contributing to increase its final aperture. The angles are also very similar during the closure phase of all the leaflets. The closure is the same for the short and long leaflets in all cases. The asymmetric leaflets ($\varepsilon = 0.5$) are the most efficient in the closure phase, closing completely at $2.24T_e$. The single leaflet and symmetric leaflets close later nearly at the same time: $2.45 \pm 0.02T_e$. The kinematics of the leaflets was very repeatable during the 60 times each run was repeated, as apparent in Fig. 6, where the opening angles of the case with $\varepsilon = 0.5$ are plotted together with their confidence intervals obtained by adding to and subtracting from the angle, θ_i, the angle standard deviation σ_i, computed at each point of the cycle and averaged over the 60 cycles ($i = 1$, 2). The case $\varepsilon = 0.5$ was chosen because it gave the highest values of the standard deviation in the acquired data set. The features of the system as a valve can be described also by the lumen that the leaflets leave open for the fluid flow, i.e. the distance between their tips, D_e. Fig. 7 shows the lumen, D_e, as a function of the non-dimensional time. The single-leaflet configuration gives the larger lumen ($0.94D$). As mentioned earlier, the shortest closure time is obtained at $\varepsilon = 0.5$. In that configuration, the lumen increases steeply, then remains nearly constant for a time interval about $0.4T_e$ long close to the maximum aperture ($0.61D$) and finally decreases to vanish at $2.24T_e$. With the symmetrical configuration, the maximum lumen attained during the cycle is the smallest ($0.52D$) though the closure time is longer than with asymmetric leaflets.

The six plots of Fig. 8 illustrate the general behaviour of the phase averaged vorticity field in the case of symmetric leaflets ($\varepsilon = 1.0$). Two almost symmetrical vortices are generated as soon as the leaflets reach their maximum angle of aperture (the leaflet position is derived automatically from the image sequence and is reported in the plots). Downstream of the vortices, lines of perturbed vorticity are observed ($t/T_e = 0.74$). These perturbations are advected by the flow in between the two vortices, which is faster than the vortices themselves, and indicate the propagation of the front of the jet. The vortices travel downstream conserving their coherence, thus suggesting that the flow remains two-dimensional. At $t/T_e = 0.89$, the vortices are still connected to the leaflets by vorticity layers, thus confirming that the pinch-off has not yet occurred. The transition to three-dimensionality can be recognized in the last plot ($t/T_e = 1.24$) where a large number of small-scale (presumably three dimensional) perturbations appear on the dipole. At that time, the dipole is apparently disconnected by the trailing vorticity layers and, in the following few instants (not shown), the vortex dipole collapses completely in a fine, three-dimensional, turbulence.

The behaviour of the vorticity field in the configuration with two non-symmetrical leaflets ($\varepsilon = 0.5$) is shown in Fig. 9. In that case, the two leaflets play a different role: they start to open simultaneously, but the small leaflet (#1 in Fig. 2) attains a lower maximum aperture, thus deviating the flow towards the large leaflet (#2 in Fig. 2), and contributing to let it reach the maximum aperture, among the presently investigated cases. Correspondingly, the two vortices start to grow at different times: at $t/T_e = 0.27$, the

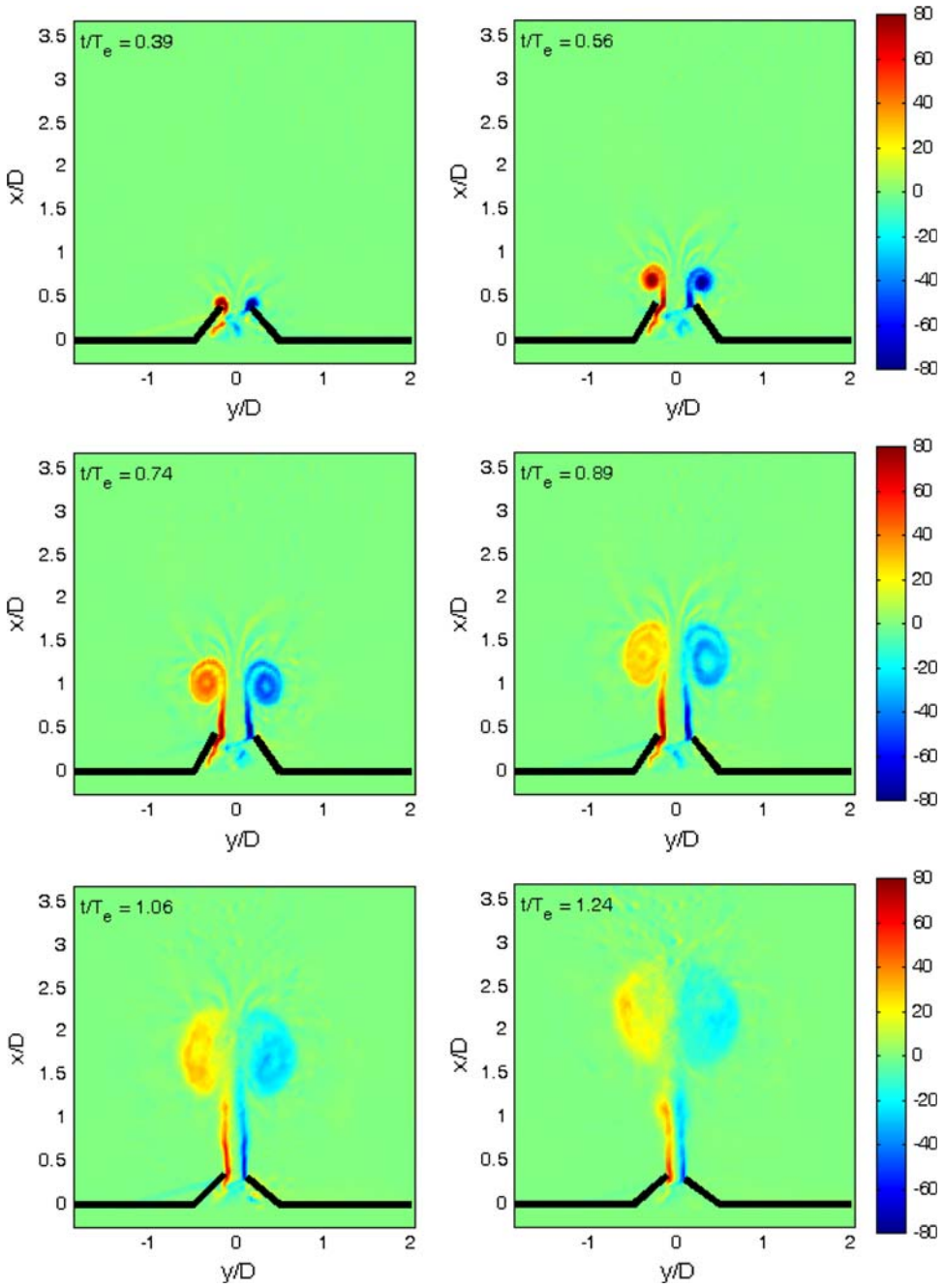

Fig. 8 Colour plot of the vorticity and leaflet positions in the symmetric configuration ($\varepsilon = 1.0$). Vorticity is non-dimensionalized by the ejection time T_e. The non-dimensional time is indicated on the *top left* of each plot

vorticity sheet begins to roll, developing from the short leaflet (leaflet #1 in Fig. 2). The vortex generated by the leaflet #2 begins to develop at $t/T_e = 0.5$. In that case, the vorticity layer rolls up at a short distance downstream of the leaflet edge. The vortex shedding is delayed due to the deviation of the flow by the short leaflet. Differently from the case $\varepsilon = 1.0$, the growth of the vortices begins just after the corresponding leaflet reaches the maximum aperture. As a consequence of the delay in the generation of vortices #1 and #2, the main features such as trajectory, vorticity and size, between them are different and also in comparison with the symmetric case. On the other hand, as for the case $\varepsilon = 1.0$, the leaflets show an intense persistent vorticity layer during the closure phase. As t/T_e becomes larger than one, the vorticity layer trailing the vortex #1 weakens noticeably, whereas the one generated by the longer leaflet is still intense. At later times ($t/T_e = 1.24$), the two-dimensional structure of the flow becomes unstable and, similarly to the case of $\varepsilon = 1.0$, there is a transition to a small-scale three-dimensional turbulence.

Also, with a single leaflet ($\varepsilon = 0.0$) the growth of the two vortices is not simultaneous. As shown in Fig. 10, the vortex #1 begins to roll up just at the beginning of the aperture phase, whereas the vortex #2 begins to roll up

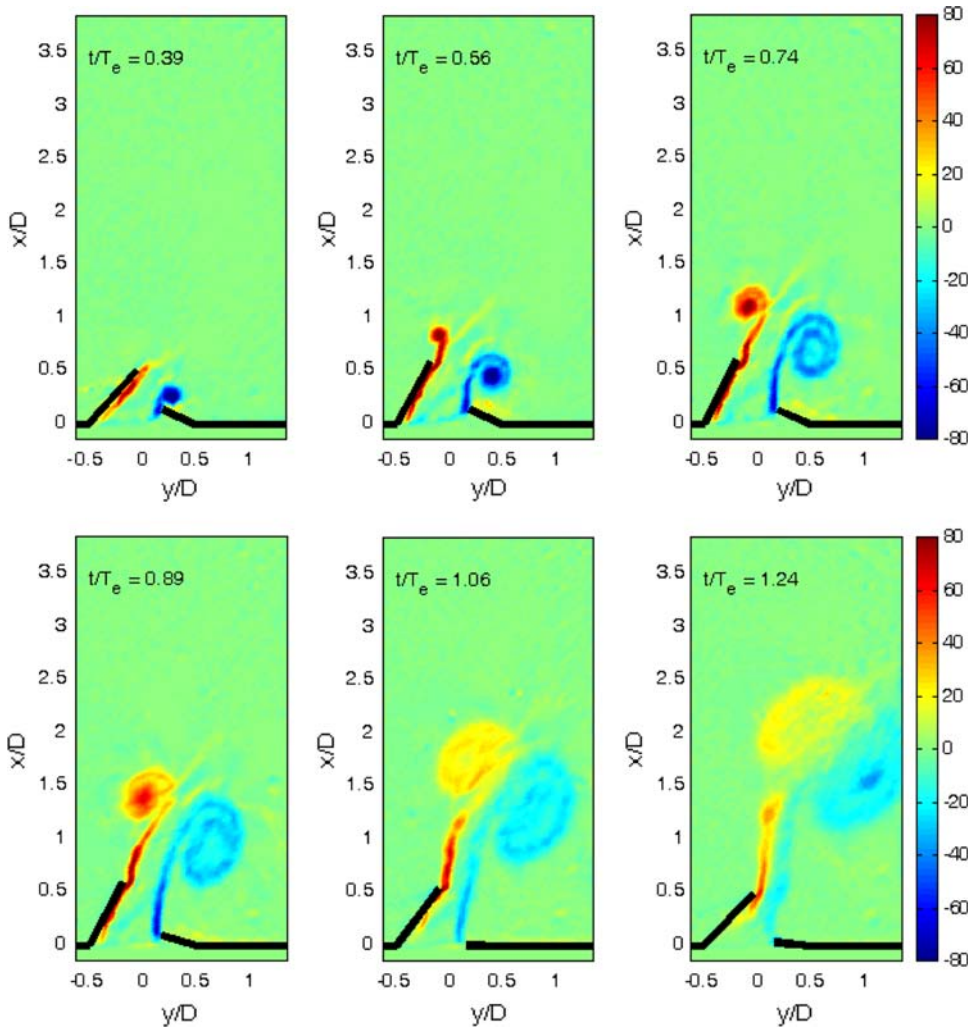

Fig. 9 Colour plot of the vorticity and leaflet positions in the non-symmetric configuration ($\varepsilon = 0.5$). Vorticity is non-dimensionalized by the ejection time, T_e. The non-dimensional time is indicated on the *top left* of each plot

at $t/T_e = 0.6$, which is later than in the case of $\varepsilon = 0.5$. At $t/T_e = 0.56$ and $t/T_e = 0.74$, two lines of vorticity in the diagonal direction of development of the jet are apparent. Even in this case, they are due to the central jet-flow that strips vorticity off the vortices and advects it downstream. However, there are significant differences both in comparison to the symmetric configuration and to the previous two-leaflet non-symmetrical condition. The vortices have lower vorticity magnitudes and presumably lower values of circulation (notice that in Figs. 8, 9, 10 the colour scale is the same). These points are considered in more detail in the next section where trajectories of the vortices are derived, and physical and geometrical quantities are measured along them. In this case, the two-dimensional structure of the flow is more stable, and at $t/T_e = 1.24$, the transition to three-dimensional turbulence has not yet occurred.

From the time evolution of the phase averaged vorticity fields, the vortex trajectories are evaluated by considering the sequence of vortex positions deriving from the minima of the invariant of the velocity gradient tensor introduced by Jeong and Hussain (1995). This quantity disregards vorticity layers while pointing out vortex core positions. In Fig. 11, the trajectories are plotted. The positions are referred to the initial position of the leaflet tips, $(x_0; y_0)$ (which is different for each configuration: $(x_0; y_0) = (0, 0)$ for $\varepsilon = 1.0$, $(x_0; y_0) = (1/6D, 0)$ for $\varepsilon = 0.5$ and $(x_0; y_0) = (1/2, 0)$ for $\varepsilon = 0.0$. With two equal leaflets ($\varepsilon = 1.0$), the trajectories of the two vortices are also symmetric. On the other hand, for leaflets of different lengths ($\varepsilon = 0.5$ and $\varepsilon = 0.0$), both vortices move towards the side of the test section that is opposite the longest leaflet. The two non-symmetric conditions show similar behaviour: with $\varepsilon = 0.5$ and $\varepsilon = 0.0$, the vortex #1 follow a straight, inclined path, whereas the vortex #2 move leftwards following the leaflet tip motion. Then, as the leaflet begins to close, and the circulation of the vortex #1 equals the one of the vortex #2, the vortices travel along straight paths that, though slightly shifted, have the orientation and the distance in common.

The time sequences of the displacement of the two vortices along the streamwise and spanwise directions are

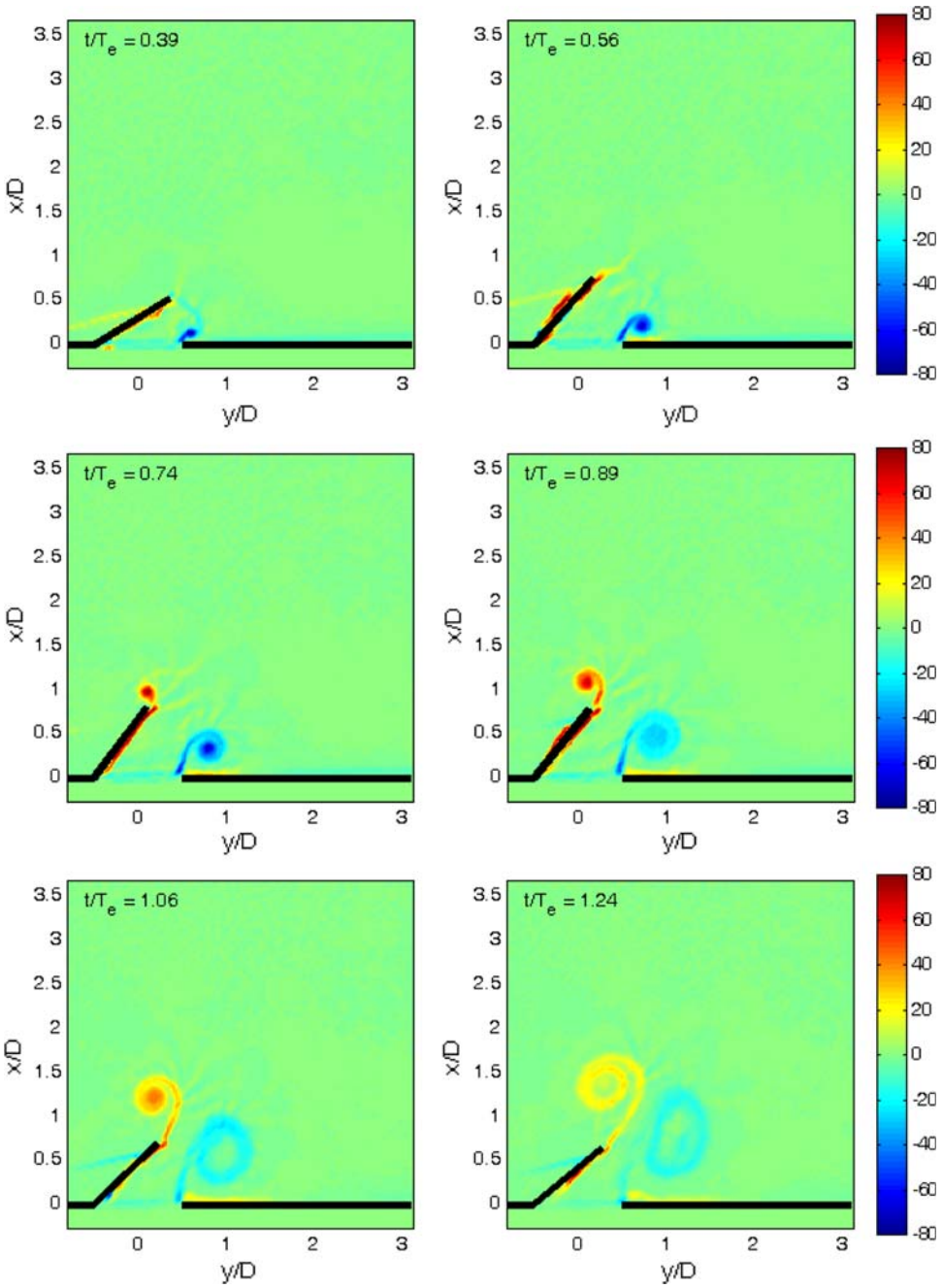

Fig. 10 Colour plot of the vorticity and leaflet positions in the single-leaflet configuration ($\varepsilon = 0.0$). Vorticity is non-dimensionalized by the ejection time, T_e. The non-dimensional time is indicated on the *top left* of each plot

shown in Figs. 12 and 13, respectively. As in Fig. 11, the coordinates are referred to the initial tip position (x_0, y_0) (the time is measured from the beginning of the cycle). For the symmetric case ($\varepsilon = 1.0$), the spanwise positions reach an almost constant value (negligible transverse velocity), while the streamwise positions increase linearly with the same slope, i.e. with the same, constant, longitudinal velocity. For the non-symmetric case $\varepsilon = 0.5$, the longitudinal positions increase in time almost as in the symmetric case (with a slightly lower velocity of the vortex #1). On the other hand, the spanwise positions and velocities are significantly different from the symmetric case; the transverse velocity is definitively not negligible, and it is about one half of the longitudinal velocity. With a single leaflet ($\varepsilon = 0.0$), the behaviour is again different: both the spanwise and streamwise positions increase with a lower slope in time in comparison to the non-symmetric case ($\varepsilon = 0.5$), so that the velocity is about one half. Thus, the vortices generated in each of the tested cases have their own peculiar behaviour depending on the details of the leaflet geometry.

In Fig. 14, the distance between the two vortices (non-dimensionalized by the orifice width, D) is presented for

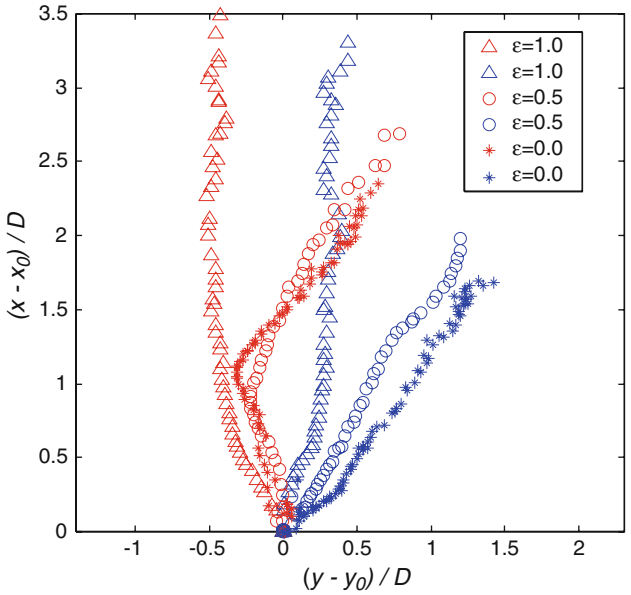

Fig. 11 Trajectories of the vortex #1 (*blue symbols*) and #2 (*red symbols*) for the tested leaflet configurations [the coordinates refer to the initial position of the vortices (x_0; y_0)]

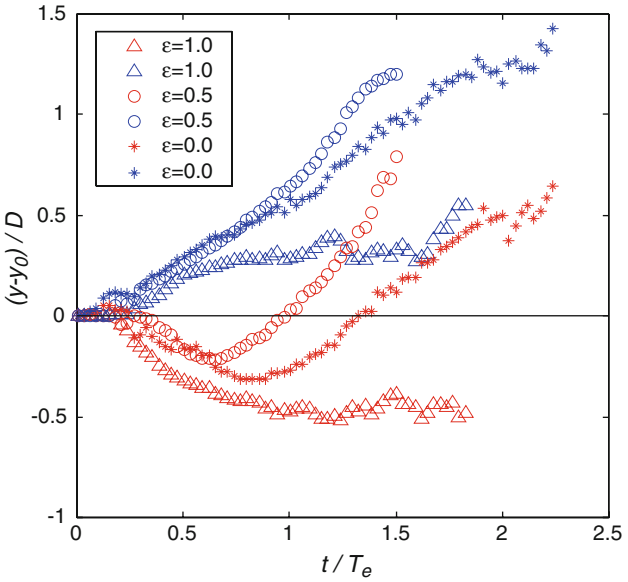

Fig. 13 Spanwise position of the vortex #1 (*blue symbols*) and #2 (*red symbols*), as a function of time for the tested leaflet configurations

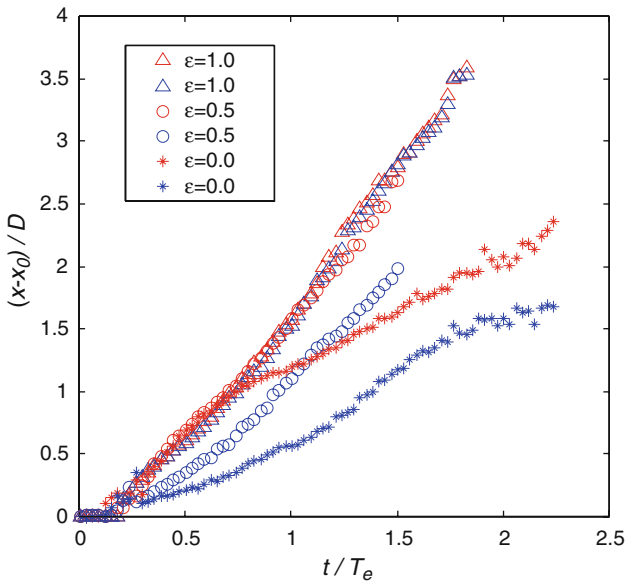

Fig. 12 Downstream distance travelled by the vortex #1 (*blue symbols*) and #2 (*red symbols*), as a function of time for the tested leaflet configurations

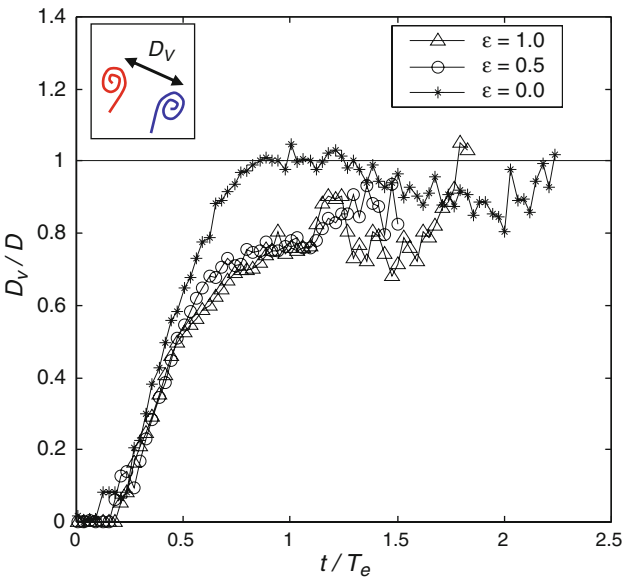

Fig. 14 Non-dimensional distance between vortices vs. non-dimensional time in the different leaflet configurations

the three configurations. The curves collapse on a single line until $0.5T_e$. Later, whereas the symmetrical ($\varepsilon = 1.0$) and non-symmetrical ($\varepsilon = 0.5$) leaflet cases exhibit the same behaviour, the single leaflet ($\varepsilon = 0.0$) reaches earlier a limiting value almost equal to the orifice width after the ejection phase. Thus, the single-leaflet configuration seems to be effective in rapidly separating the two vortices. This seems to be the effect of a wider effective opening of the single-leaflet orifice compared to the other configurations. The larger separation distance between the vortices determines, in turn, a lower vortex propagation velocity as observed earlier.

In Fig. 15, the core diameters of the vortex #1 and #2 are plotted (diameters are evaluated as the diameter of the iso-vorticity line corresponding to 1/4 of the peak level).

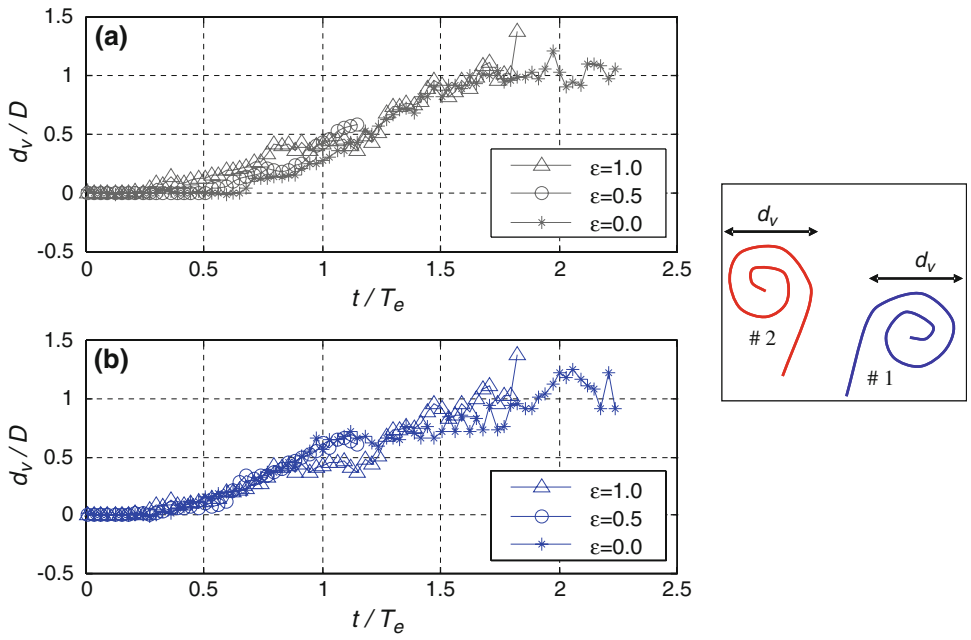

Fig. 15 Diameter of the core of the vortex #1 (*blue plots*) and #2 (*red plots*) in the different leaflet configurations

The #2 vortex core diameters are shown in Fig. 15a. For the non-symmetrical conditions, they begin to develop earlier in comparison to the #1 vortex cores, as already observed in Figs. 9 and 10. The trend is the same for all conditions, at least for $t/T_e < 1.4$. On the other hand, the diameters of the vortex #1 (Fig. 15b) increase with a significant delay in the non-symmetric conditions ($\varepsilon = 0.5$ and $\varepsilon = 0.0$). Thus, at a given time, the diameter of the vortex core #2 generated in symmetric conditions is usually larger than those in non-symmetric configurations and of the same order of the diameter of the core of the vortex #1. The diameters of vortices #2 in non-symmetric conditions are only 1/3 to 1/2 of the diameters of the vortices #1.

All these observations indicate that the longest leaflet late opening drives the two vortices towards one side (rather than straight ahead) originating them at different times and with different size (at least initially). Indeed, for all conditions the limiting values of diameters are similar (about one orifice width).

Vorticity and circulation of vortices #1 and #2 along their trajectories are reported in Figs. 16 and 17, respectively. Vorticity is evaluated as the average of the values over the region delimited by the diameters presented in Fig. 15. The plots show common behaviour, which is closely related to the piston velocity: the vorticity increases during the accelerated ejection, reaching the maximum value at about $t/T_e = 0.5$. During the decelerated ejection and later, the vorticity decreases smoothly to zero as the vortex becomes unstable and breaks in three-dimensional turbulence. This behaviour is delayed for the vortices #2 in the non-symmetrical cases $\varepsilon = 0.5$ and $\varepsilon = 0.0$ about 0.4

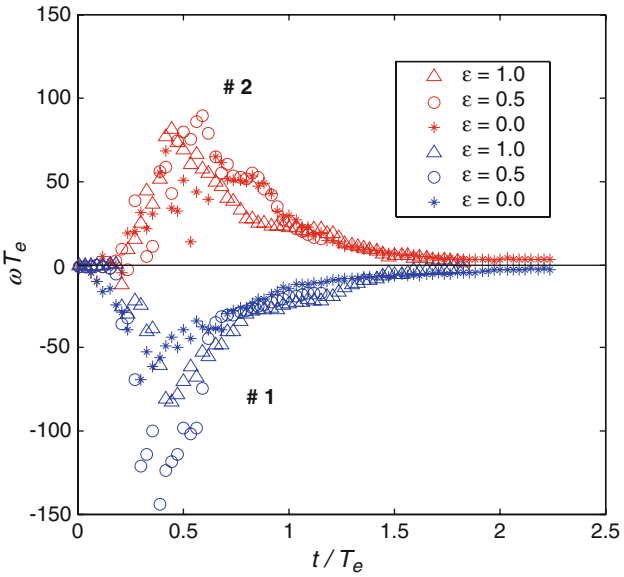

Fig. 16 Non-dimensional average vorticity of vortex #1 (*blue symbols*) and #2 (*red symbols*) as a function of the non-dimensional time in the tested leaflet configurations

t/T_e later. The main difference between the investigated configurations is in the maximum vorticity value attained at the end of the accelerated ejection. The peak vorticity of the vortex generated by the longest leaflet is about the same in all the tested configurations, whereas the vortex #1, generated by the shortest leaflet, exhibits the maximum peak vorticity when $\varepsilon = 0.5$. The vorticity is well balanced between the two vortices in symmetric conditions. Lower values are observed for the single-leaflet case ($\varepsilon = 0.0$) for the both positive and negative maximum vorticities.

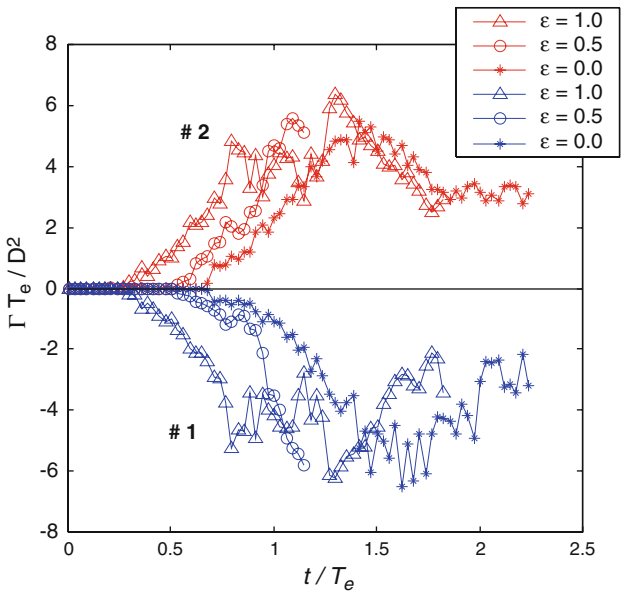

Fig. 17 Non-dimensional circulation of vortex #1 (*blue symbols*) and #2 (*red symbols*) as a function of non-dimensional time

The circulation has been evaluated using Stokes theorem, and it is plotted in Fig. 17. Due to the very small vorticity values (Fig. 16) and vortex core diameters (Fig. 15), it is almost zero up to the middle of the leaflet aperture phase and starts to increase firstly in the symmetric case ($t/T_e \approx 0.3$) and later in the non-symmetric case ($\varepsilon = 0.5$) and the single-leaflet case ($\varepsilon = 0.0$) ($t/T_e \approx 0.5$ and $t/T_e \approx 0.7$, respectively). The early increase in the circulation in the symmetric configuration may be related to the lower lumen, D_e, generating, locally, higher velocities in between the leaflets. An opposite effect is observed with the single leaflet, which gives the large maximum lumen. From there on, the growing rate and the limiting values are similar in all the conditions; slight asymmetries are observed for $\varepsilon = 0.5$ and $\varepsilon = 0.0$ indicating delayed growth of circulation of the vortex #1 (negative values) compared to #2 (positive values); however, the final values of the circulation are symmetric, as demonstrated by the final straight path of the vortices.

4 Remarks and conclusions

In the present work, measurements of the velocity field downstream a two-dimensional jet have been performed by means of robust image velocimetry (RIV). The jet-flows through a rectangular orifice equipped with moving leaflets of different widths, aiming to give some insight into the fluid mechanics of a phenomenon that has salient features in common with flows generally found in nature, such as in the flow through heart valves or in aquatic animal jet propulsion.

A piston, controlled by a personal computer, drives the flow that, in turn, forces the leaflets to open. The stroke volume and period have been selected in order to reproduce Reynolds and Strouhal numbers in the range of typical biological conditions (e.g. in the case of the mitral valve in the human heart). As the flow develops through the orifice, the leaflets open and generate a couple of counter-rotating vortices moving downstream.

In the symmetric case, the two leaflets open similarly, and the two generated vortices move straight ahead. The resulting transverse velocities of the vortices are almost zero, while the longitudinal velocities are relatively high. As expected, the two vortices have almost the same size, vorticity and circulation.

In the two leaflets, non-symmetric case, one being twice as wide as the other, the aperture angles and times of the two leaflets are strongly different, which result in the two vortices moving towards one side of the field. The resulting transverse velocities are a significant fraction of the longitudinal one (about one half), which is also about the same as in the symmetrical case. One of the two vortices (the one opposite to the large leaflet) develops before the other, resulting in a larger size and different vorticity. In spite of their different development, the two vortices attain nearly the same circulation at the end of their formation; thus, they move along straight, parallel lines.

In the case with a single leaflet, the aperture angle is lower than the previous ones, and there is some delay in the aperture. Similarly to what described earlier, the resulting couple of vortices moves towards one side of the field. However, the resulting vortex propagation velocity is lower than in the two-leaflet non-symmetrical case with two leaflets because the distance between the vortices is larger. Even in this case, the vortex developing on the side opposite to the leaflet is generated before the other and increases to a larger size. On the other hand, the circulations are about the same after the initial stage of development. Therefore, similarly to the other cases, the vortices travel along straight, parallel paths.

In conclusion, the asymmetric two-leaflet configuration seems to accomplish better the advantages of the symmetric configuration (short opening time) and those of the single-leaflet configuration (large opening angle), giving an intermediate maximum lumen that, on the other hand, is maintained for a 0.4 T_e long interval. At the same time, it minimizes the disadvantages of both the configurations, exhibiting the shortest closure time among the configuration tested. Though the configuration investigated is very simplified, and a small set of conditions have been tested, these results suggest that the motivation of asymmetries found in nature could be the optimization (accordingly with the numerical findings of Pedrizzetti and Domenichini (2007)). For example, the different sizes of the leaflets of

the human mitral valve could be the most favourable for their function.

Acknowledgments This work has been partially funded by the Italian Ministero dell'Università e della Ricerca. PRIN project 2006—prot. 2006087719.

References

Akutsu T, Imai R, Deguchi Y (2005) Effect of the flow field of mechanical bileaflet mitral prostheses on valve closing. J Artif Organs 8:161–170

Anderson EJ, Grosenbaugh MA (2005) Jet flow in steadily swimming adult squid. J Exp Biol 208:1125–1146

Bolzon G, Zovatto L, Pedrizzetti G (2003) Birth of three-dimensionality in a pulsed jet through a circular orifice. J Fluid Mech 493:209–218

Brucker C, Steinseifer U, Schroder W, Reul H (2002) Unsteady flow through a new mechanical heart valve prosthesis analysed by digital particle image velocimetry. Meas Sci Technol 13:1043–1049

Cooke J, Hertzberg J, Boardman M, Shandas R (2004) Characterizing vortex ring behaviour during ventricular filling with Doppler echocardiography: an in vitro study. Ann Biomed Eng 32(2):245–256

Dabiri JO, Gharib M (2005a) Starting flow through nozzles with temporally variable exit diameter. J Fluid Mech 538:111–136

Dabiri JO, Gharib M (2005b) The role of optimal vortex formation in biological fluid transport. Proc. R. Soc. B 272:1557–1560

Dasi LP, Ge L, Simon HA, Sotiropoulos F, Yoganathan AP (2007) Vorticity dynamics of a bileaflet mechanical heart valve in an axisymmetric aorta. Phys Fluids 19(6):17 (067105)

De Tullio MD, Cristallo A, Balaras E, Verzicco R (2009) Direct numerical simulation of the pulsatile flow through an aortic bileaflet mechanical heart valve. J Fluid Mech 622:259–290

Falchi M, Querzoli G, Romano GP (2006) Robust evaluation of the dissimilarity between interrogation windows in image velocimetry. Exp Fluids 41(2):279–293

Gharib M, Rambod E, Shariff K (1998) A universal time scale for vortex ring formation. J Fluid Mech 360:121–140

Grande KJ, Cochran RP, Reinhall PG, Kunzelman KS (1998) Stress variations in the human aortic root and valve: the role of anatomic asymmetry. Ann Biomed Eng 4(26):534–545

Jeong J, Hussain F (1995) On the identification of a vortex identification. J Fluid Mech 285:69–94

Kaminsky R, Dumont K, Weber H, Schroll M, Verdonck P (2007) PIV validation of blood-heart valve leaflet interaction modelling. Int J Artif Organs 30(7):640–648

Pedrizzetti G, Domenichini F (2006) Flow-driven opening of a valvular leaflet. J Fluid Mech 569:321–330

Pedrizzetti G, Domenichini F (2007) Asymmetric opening of a simple bi-leaflet valve. Phys Rev Lett 98(21):1–4 (214503)

Pullin DI (1979) Vortex ring formation at tube and orifice openings. Phys Fluids 22(3):401–403

Saffman PG (1970) The velocity of viscous vortex rings. Stud Appl Math 49:371

Shariff K, Leonard A (1992) Vortex rings. Ann Rev Fluid Mech 24:235–279